RESEARCH ARTICLE

INTERNATIONAL RESEARCH JOURNAL OF MULTIDISCIPLINARY TECHNOVATION

Asian Research Association

DOI: 10.54392/irjmt26322

Growth, Third-Order Nonlinear Optical, Thermal and Quantum Chemical Investigation of L-Ornithine Monohydrochloride Single Crystals

N. Saranya [a, b], R. Karunathan [a, *], P. Vidhya [c], S. Bhuvaneswari [d]

[a] Department of Physics, Dr.N.G.P. Arts and Science College, Coimbatore-641048, Tamil Nadu, India.
[b] Department of Physics, Jansons Institute of Technology, Karumathampatti, Coimbatore-641659, Tamil Nadu, India.
[c] Department of Science and Humanities (Physics), Nehru Institute of Engineering and Technology, Coimbatore-641105, Tamil Nadu, India
[d] Department of Physics, KPR Institute of Engineering and Technology, Coimbatore-641407, Tamil Nadu, India
* Corresponding Author Email: drkarunathan@drngpasc.ac.in

DOI: https://doi.org/10.54392/irjmt26322

Received: 17-02-2026; Revised: 12-05-2026; Accepted: 18-05-2026; Published: 26-05-2026

Abstract: Single crystals of L-ornithine monohydrochloride (LOHCL) were successfully synthesized at ambient temperature using the slow evaporation technique and systematically investigated through complementary experimental and computational techniques to assess their relevance for nonlinear-optical and optoelectronic applications. Single-crystal and powder X-ray diffraction confirmed the formation of the known monoclinic LOHCL phase with good crystallinity. UV–visible spectroscopy revealed high transparency across the visible range with a lower absorption edge near 223 nm, indicating favourable optical transmission. Thermal analyses by TGA, DTA and DSC indicated that the material maintains thermal stability up to approximately 255 °C before undergoing a major transformation. FT-IR and FT-Raman spectra supported the ionic amino-acid hydrochloride structure and were consistent with the diffraction results. Photoluminescence measurements exhibited a blue emission band centred at 474 nm. Z-scan analysis established a positive nonlinear refractive index of 5.056×10^{-8} cm² W^{-1} and a nonlinear absorption coefficient of 0.06×10^{-4} cm W^{-1}, confirming appreciable third-order nonlinear optical characteristics. DFT calculations using the B3LYP/6-311++G(d,p) level further clarified the electronic configuration, charge distribution, thermodynamic behaviour and intermolecular interactions. The calculated HOMO–LUMO energy gap was found to be 3.00 eV. The combined findings support LOHCL for advanced photonic, laser-based and frequency-conversion technology platforms.

Keywords: Nonlinear Optical Properties, Solution Growth, FT-Raman, L-Ornithine Monohydrochloride, DFT, Density Functional Theory, Z-Scan.

1. Introduction

Organic nonlinear optical (ONLO) materials continue to attract significant interest because they integrate strong optical nonlinearity, ultrafast electronic response, low dielectric constant, and extensive structural tunability within a single molecular framework [1-3]. In contrast to conventional inorganic crystals, organic and semi-organic systems permit molecular-level modulation through functional group substitution, intermolecular hydrogen bonding, and charge-transfer interactions, all of which directly influence electronic polarization, optical susceptibility, and transparency [4]. Recent investigations have identified amino acid-based crystals as particularly promising candidates for photonic and optoelectronic applications because their zwitterionic configuration promotes strong molecular dipoles and facilitates non-centrosymmetric crystal packing, a critical structural requirement for efficient second harmonic generation (SHG) and related nonlinear optical processes [5]. Compared with purely inorganic NLO systems, amino acid crystals additionally exhibit superior optical damage tolerance, lower processing cost, and facile solution-growth characteristics, thereby enhancing their suitability for integrated photonic and laser-driven device architectures [6].

Current research in nonlinear optical materials has shifted beyond the isolated enhancement of SHG efficiency toward the development of systems capable of simultaneously maintaining optical transparency, thermal robustness, mechanical stability, and efficient electronic delocalization under operational conditions. In organic NLO materials, nonlinear polarization predominantly originates from intramolecular charge-

transfer processes and π-electron delocalization pathways that facilitate rapid redistribution of electron density under external electromagnetic excitation [7]. Molecules containing donor–acceptor configurations generally exhibit enhanced hyperpolarizability because the reduced energetic barrier for electron migration strengthens induced dipole formation during optical excitation [8]. In addition, theoretical studies have demonstrated that hydrogen-bond-assisted electronic coupling and molecular packing density critically regulate charge transport pathways, local polarization fields, and optical susceptibility in amino acid crystals [9, 10]. These observations establish that nonlinear optical efficiency is governed not only by molecular electronic structure but also by crystal packing-induced electronic interactions and defect-mediated polarization behaviour.

Among amino acid-derived NLO systems, L-ornithine-based materials have become an attractive candidate owing to extensive hydrogen-bonding network, favourable dielectric characteristics, and broad optical transparency window. Previous crystallographic studies have already established the structure of L-ornithine hydrochloride and its hydrogen-bonded ionic arrangement [11, 12]. Subsequent crystallographic refinement studies have also treated this salt as a reference system [13]. Accordingly, the novelty of the present work is not the first synthesis or first structure determination of LOHCL; rather, it lies in combining crystal growth, optical and thermal characterization, Z-scan analysis, and DFT-based electronic-structure evaluation within a single study. Previous optical studies reported that LOHCL crystallizes in the non-centrosymmetric monoclinic space group P21 and exhibits SHG activity relative to KDP [14, 15]. Nevertheless, a consolidated study linking diffraction-verified phase formation with vibrational, optical, thermal and quantum-chemical analysis remains limited.

A major limitation in many previously reported amino acid crystals is the inadequate understanding of how frontier molecular orbitals, intermolecular charge-transfer interactions, and electronic delocalization collectively govern macroscopic nonlinear optical behaviour. Recent DFT investigations have demonstrated that HOMO–LUMO energy separation, molecular electrostatic potential distribution, and first-order hyperpolarizability parameters critically determine charge-transfer efficiency, electronic excitation behaviour, and nonlinear polarization response in organic crystalline systems. Furthermore, Natural Bond Orbital (NBO) analysis has proven effective for identifying donor–acceptor stabilization pathways and quantifying electron delocalization mechanisms arising from intermolecular interactions and hydrogen-bond-assisted charge redistribution [16]. Consequently, the integration of experimental characterization with quantum chemical modelling provides a more reliable framework for correlating molecular electronic structure with macroscopic optical performance.

Considering these factors, the current work concentrates on the growth and comprehensive analysis of L-ornithine monohydrochloride crystals through combined experimental and computational approaches. The prepared crystals were analysed using X-ray diffraction, FT-IR, FT-Raman, UV–visible spectroscopy, photoluminescence analysis, thermal measurements, and Z-scan techniques to evaluate their structural integrity, electronic transitions, thermal behaviour, and nonlinear optical response. In parallel, DFT calculations were carried to understand the electronic structure, frontier molecular orbitals, charge distribution, thermodynamic stability, and intermolecular interaction mechanisms associated with the LOHCL system. By correlating spectroscopic observations with quantum chemical analysis, this study establishes a detailed structure–property relationship governing the optoelectronic and nonlinear optical behaviour of LOHCL crystals, thereby assessing their potential for advanced photonic and frequency-conversion device applications.

2. Methodology

2.1. Crystal Growth

When LOHCL was crystallized at ambient temperature using the slow evaporation method, the resulting crystals were of high quality. To produce LOHCL, pure l-ornithine (99%, from Merck) of 10 g and high-purity hydrochloric acid solution of 0.5 ml were mixed in 80ml double distilled water and stirred together for 6 hours at room temperature. Another beaker was filled with the filtered solution, and a perforated lid was placed over it. Solubility data showed that at 40^{o}C the solution was saturated, causing nucleation of seed crystals. Needle-shaped single crystals of LOHCL, measuring 19 x 11 x 3 mm^3, were produced after 20 days and a sample crystal is shown in Figure 1.

2.2 Characterization Techniques

A comprehensive characterization of the grown LOHCL crystals was undertaken to examine phase formation, unit-cell parameters, vibrational features and thermal stability. Single-crystal X-ray diffraction was used to obtain the unit-cell parameters, and powder X-ray diffraction was used to verify phase purity and crystallinity. FT-IR and FT-Raman spectroscopy were used only as supportive vibrational analyses and not as the sole proof of crystal identity. A double-beam Fourier-transform infrared (FT-IR) spectrometer (Shimadzu) was used to record the infrared spectrum. A confocal micro-Raman spectroscope in the frequency range 500 to 3500 cm−1 was used to investigate the vibrational modes. Crystals were dissolved in ethanol and scanned in the range 200–1100 nm on a PerkinElmer Lambda 365 spectrophotometer. Thermal stability analysis was performed using a Hitachi STA7000 instrument for TGA, DTA and DSC.

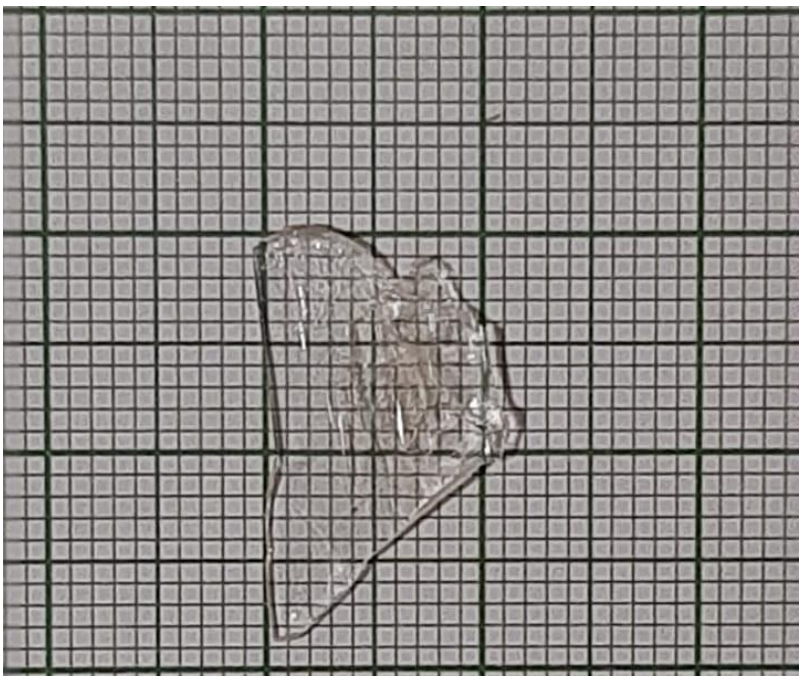

Figure 1. The grown crystal of the compound L-Ornithine monohydrochloride

A PerkinElmer Spectrum Model FL 1.3.0 was used to record the photoluminescence spectrum. The nonlinear optical response was evaluated using the Z-scan technique.

2.3 Computational Details

The structural and vibrational aspects of LOHCL at the molecular scale were analyzed by performing DFT calculations using the software package Gaussian 09W [17]. The Hartree–Fock (HF) method was employed, as well as a version of B3LYP that combines HF and DFT. Because the molecule can be polarized, different techniques employing the 6-31++G and 6-311++G(d,p) basis sets were explored. The molecular structure of LOHCL was constructed and geometrically optimized at the B3LYP/6-311++G(d,p) level of theory. To gain deeper insight into the electronic interactions present within the LOHCL system, Natural Bond Orbital (NBO) analysis was carried out using DFT calculations at the B3LYP/6-311++G(d,p) level [18].

3. Results and Discussion

3.1 X-Ray Diffraction Analysis

The as-grown crystal was characterized at room temperature using both single-crystal and powder X-ray diffraction techniques. The analysis confirmed that LOHCL belongs to the monoclinic crystal system with lattice parameters of a = 9.948 (2) Å, b = 8.005 (3) Å, c = 4.992 (3) Å, β = 95.67°, and a unit-cell volume of 395.59 Å³. The powder XRD pattern of the prepared crystal, recorded over 10–80°, is presented in Figure 2. The sharp Bragg reflections confirm good crystallinity, and the observed peaks are consistent with previously reported diffraction data for L-ornithine hydrochloride [11, 12]. These results support assignment of the grown material as the known LOHCL phase and indicate the absence of obvious secondary phases within the detection limit of the measurement.

3.2 FT-IR Spectral Study

FT-IR spectroscopy was used to support the vibrational analysis of the diffraction-identified LOHCL phase (Figure 3). The broad band at 3426 cm−1 is associate with overlapping N–H and O–H stretching vibrations. The band at 1628 cm−1 is ascribed mainly to NH3+ deformation together with asymmetric COO− stretching. The band near 1329 cm−1 agrees to the symmetric stretching of the carboxylate group, while features in the 1250–1000 cm−1 region arise from C–N stretching and related skeletal vibrations. The band at 934 cm−1 is attributed to a C–C skeletal vibration. The lower-wavenumber bands at 782, 757 and 669 cm−1 are more appropriately described as COO− out-of-plane/lattice modes associated with the ionic crystal environment; they should not be interpreted as covalent C–Cl vibrations. Overall, the FT-IR features are consistent with the previously reported amino-acid hydrochloride salt structure of LOHCL (table 1).

3.3 FT-Raman Analysis

Raman spectroscopy was used as a complementary vibrational probe for LOHCL (Figure 4). The observable bands near 1351, 1786, 2947 and 3079 cm−1 are consistent with NH/C–H stretching and carboxylate-related modes reported for amino-acid hydrochloride salts. Features in the 1350–1800 cm−1 region can be assigned to COO− vibrations, NH3+ deformation and CH2 modes, whereas the low-

wavenumber region (<400 cm−1) is associated mainly with lattice vibrations. Because X-ray diffraction provides the primary structural verification in this work, the Raman spectrum is interpreted here qualitatively as supportive evidence rather than as a standalone structural proof.

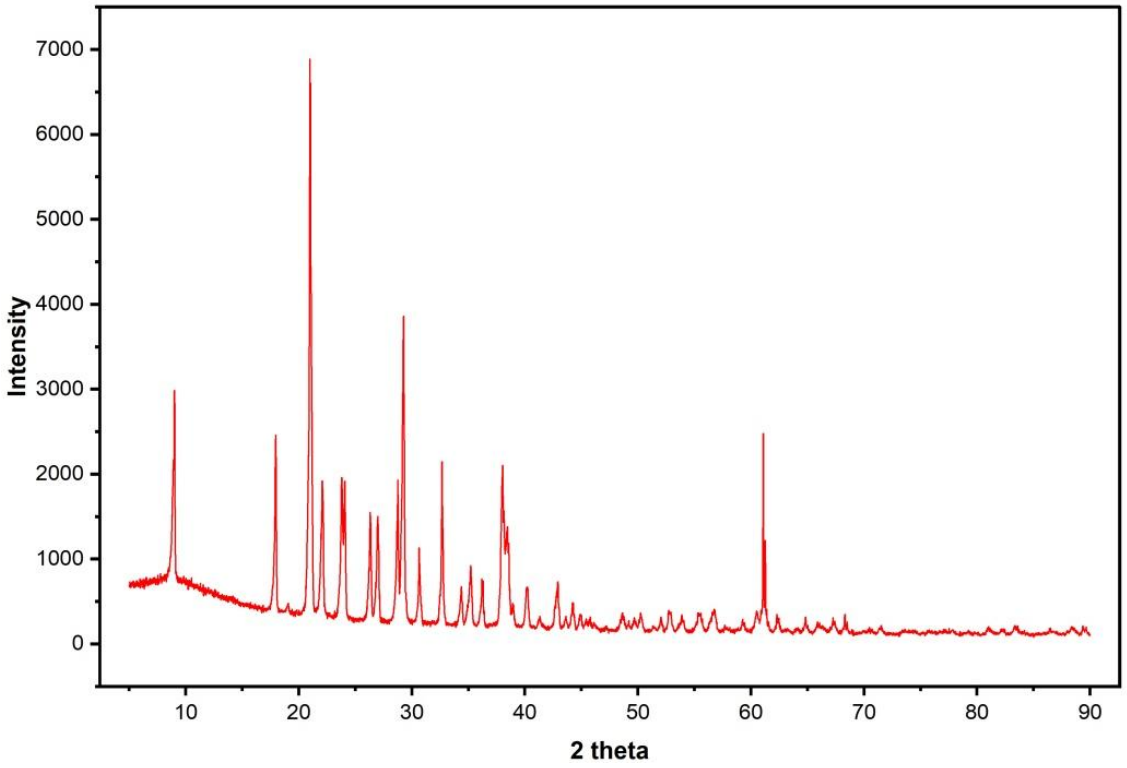

Figure 2. Powder X-ray diffraction pattern of LOHCL

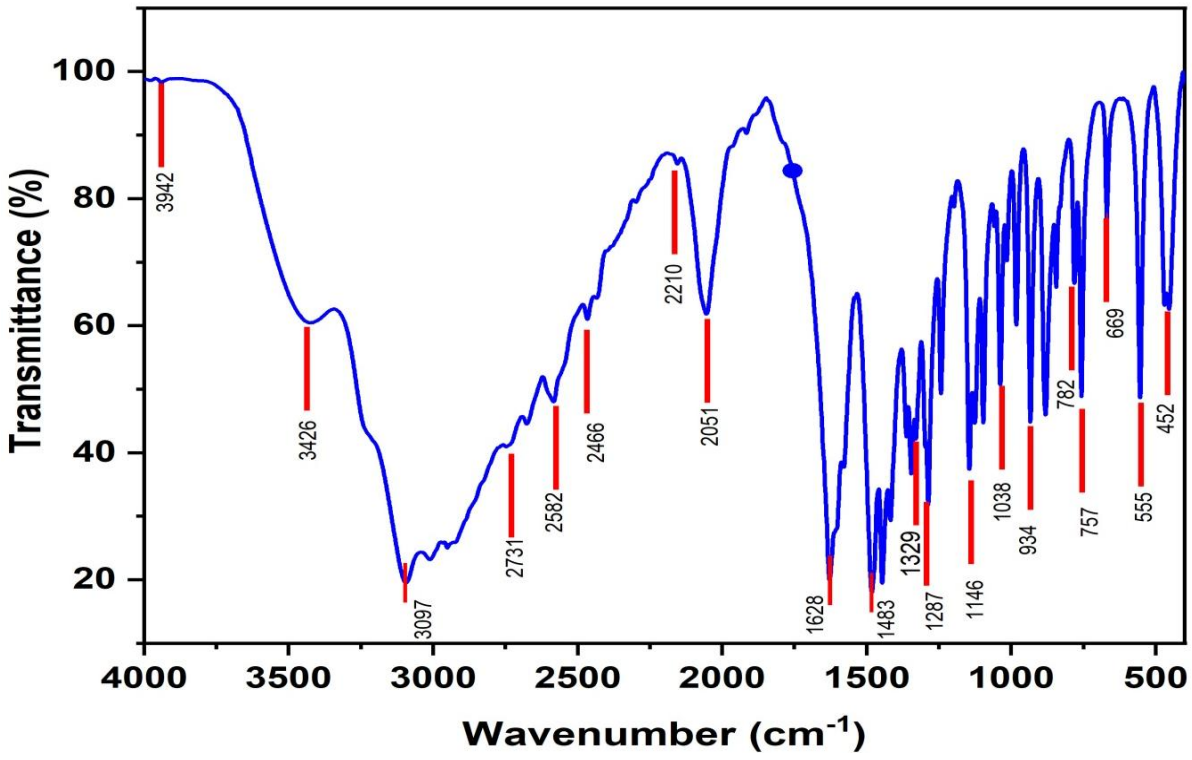

Figure 3. FT-IR Analysis of LOHCL

Table 1. Experimental and Theoretical Vibrational Assignments of LOHCL

Vibrational Assignment	Experimental		Calculated Frequencies at B3LYP/6-311++ G(d,p) (cm^{-1})
	FTIR (cm^{-1})	FT-RAMN (cm^{-1})	
N–H and O–H stretching vibrations	3942, 3426	3480, 3743	3725, 3649
NH_3^+ stretching and aliphatic C–H stretching	3097	2947, 3079	3088
Combination and overtone modes	2731, 2582, 2466, 2210	2481, 2156	2624,2351
Asymmetric stretching of carboxylate group	1628	1786	1675
NH_3^+ bending vibration	1483	1351	1485
Symmetric stretching of carboxylate group	1329	1351	1376
C–N stretching vibration	1287	1351	1247
C–O stretching vibration	1146	-	1196
C–N / C–O deformation modes	1038	-	1072
C–C skeletal vibrations	934	-	963
COO^- out-of-plane bending / lattice contribution	782, 757, 669	122	796
Lattice and skeletal deformation vibrations	555, 452	<400	493,395

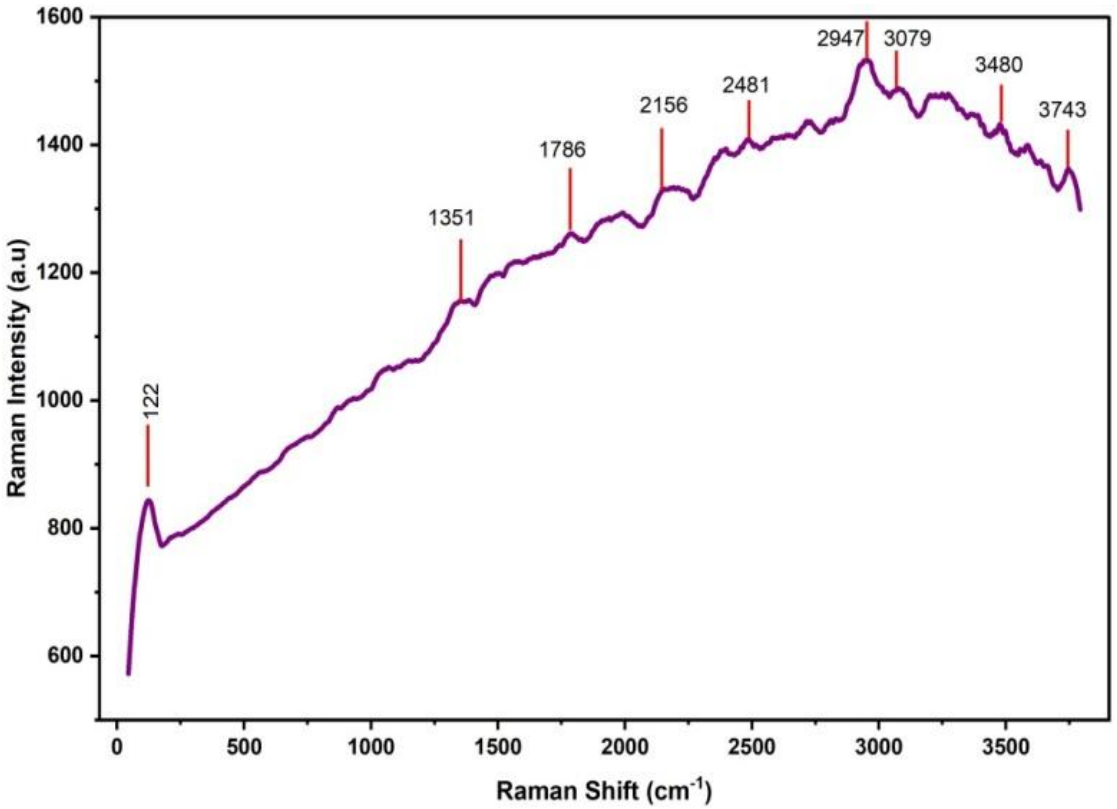

Figure 4. FT-Raman Analysis of LOHCL

3.4 UV-Visible Spectrum

The optical transmission capability of LOHCL crystals for optoelectronic applications was examined using UV–visible spectroscopy. A thin crystal specimen was recorded in the wavelength range of 200–1100 nm using a PerkinElmer Lambda 365 spectrophotometer (Figure 5). The obtained spectrum revealed excellent transparency across the visible region (380–700 nm), with a lower cut-off wavelength around 223 nm. The minimal absorption observed in the visible range indicates that the crystal is well suited for efficient optical transmission applications. The present result is broadly consistent with earlier optical studies on LOHCL and related organic crystals [8, 19 and 20]. The very low absorption observed across the visible region indicates minimal loss of transmitted light, highlighting the potential of LOHCL for advanced optoelectronic studies and related optical device applications.

3.5 Thermal Analysis

To examine the thermal behaviour of LOHCL, TGA, DTA and DSC measurements were performed in a gas atmosphere using a Hitachi STA7000 instrument. A 10.2925 mg sample was heated from 30 °C to 810 °C at 5.00 °C min−1. The thermogram shows that the crystal remains stable up to about 255 °C, followed by a single major transformation step. The corresponding endothermic event near 255 °C is consistent with the melting/decomposition behaviour of the salt. Because the key thermal information for the present study is the stability limit, the full TG/DTA/DSC trace is provided in Figure S1.

3.6 Photoluminescence Studies

The Photoluminescence measurements were made by PerkinElmer Spectrum Model FL 1.3.0. A Xenon lamp is used in the sample compartment module which functions at 450 W. The photoluminescence emission spectrum of the LOHCL crystal was measured over the wavelength range of 380–500 nm using an excitation wavelength of 310 nm. The recorded PL spectrum displayed an intense and well-defined emission peak centred at 474 nm, indicating prominent blue light emission. In Figure 6, the PL [photoluminescence] spectrum collected from the title material is shown. The observed luminescence behaviour indicates efficient radiative recombination and suggests the suitability of LOHCL crystals for optoelectronic and photonic applications.

3.7 Z-Scan Studies

The Z-scan approach is used to examine the nonlinear optical features of prepared crystals of LOHCL [15]. With this approach, both n_2 and β can be calculated. In nonlinear optics, the important nonlinear effect is explained by the third-order nonlinear susceptibility which is why n_2 is related to β. The Z-scan method consists of scanning a polished LOHCL crystal (4 x 4 x 1 mm) along its length in the direction in which the laser light passes through the focal point.

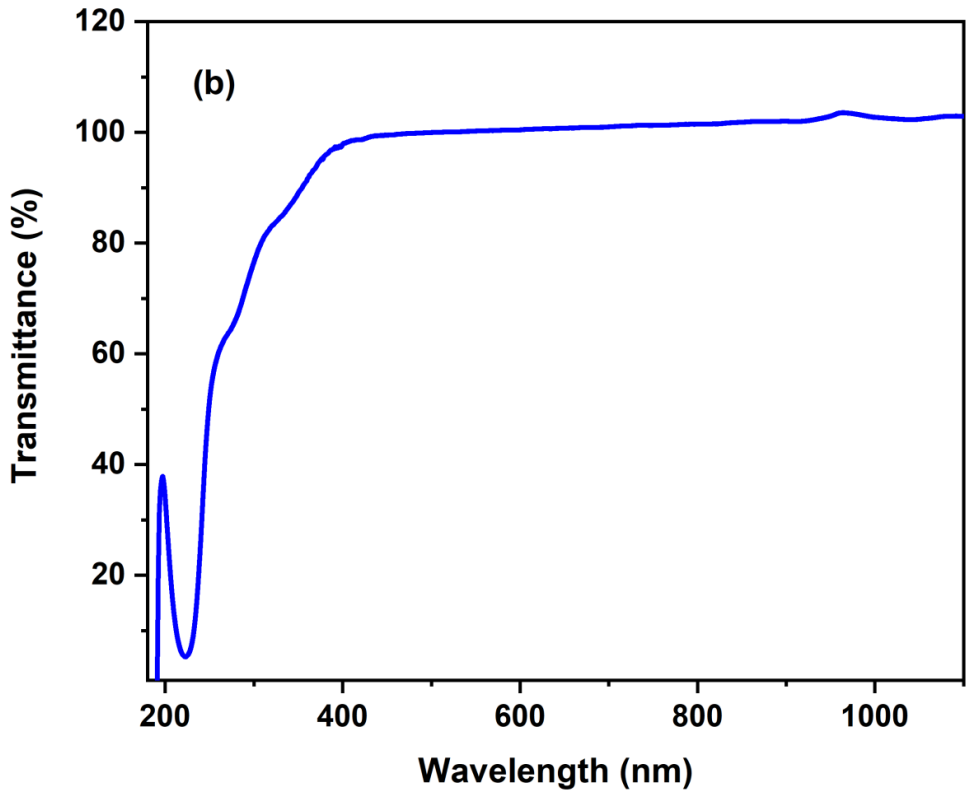

Figure 5. UV-vis transmission spectrum of LOHCL

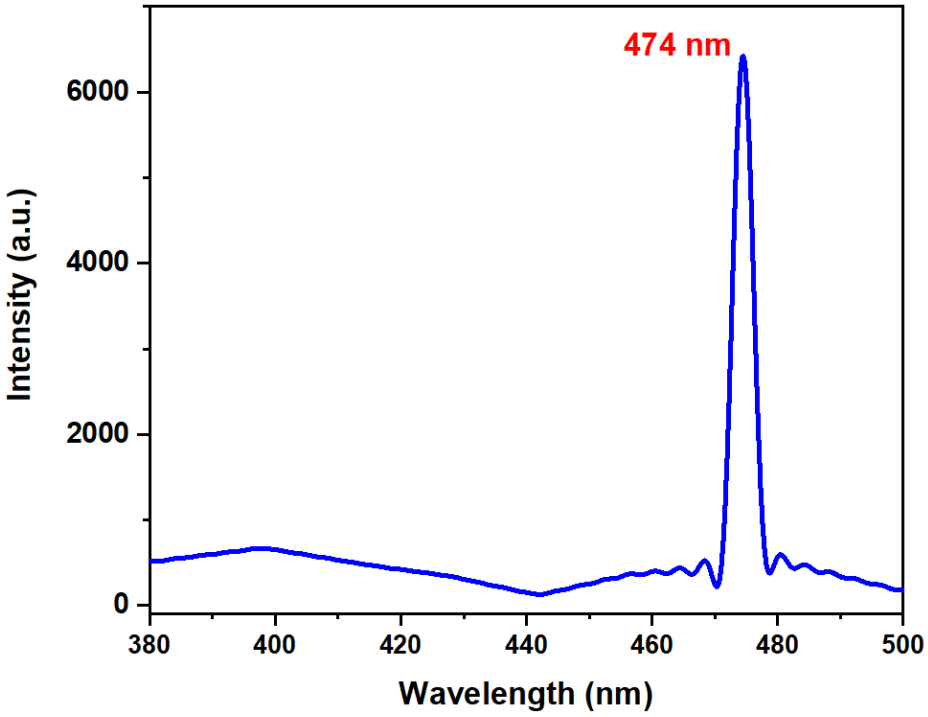

Figure 6. Photoluminescence spectrum of LOHCL

Most measurements are performed using either the open-aperture or closed-aperture Z-scan method. Direct observation of or photographing the transmitted light is used to visualize the optical absorption in open-aperture Z-scan. It gives explanations about the β structure. In contrast to an open-aperture Z-scan, phase shifts in the light are the sole measurements in closed-aperture Z-scan. This is where the light rays shining through the substance are gathered on a small disc to get the value of n_2. Z-scan measurements in this experiment were done using a CW Nd-YAG laser. The sample was positioned along the z-axis one layer at a time and the intensity of the light was checked after each layer at the far-field position [21]. The measured normalized transmittance (T) for both open-aperture and closed-aperture Z-scan configurations is presented in Figure 7(a) & (b). The n_2 and β values are calculated from these data for the LOHCL crystals.

ΔT p-v (the transmittance difference between peak and valley) can be written as a function of $|\Delta\phi|$:

$$\Delta T_{p-v=0.406\,(1-S)^{0.25}\,|\Delta\phi|} \quad (1)$$

Δϕ denotes the phase shift of light with focus in the image and S is the aperture transmittance, this is calculated using the formula

$$S = 1 - exp[\frac{-2r_a^2}{\omega_a^2}] \quad (2)$$

The aperture radius is denoted by r_a, while ω_a represents the beam radius at the aperture position. The third-order nonlinear refractive index is related to the on-axis phase shift through the following expression

$$n_2 = \frac{\Delta\phi}{kI_0L_{eff}} \quad (3)$$

Where k=2π/λ, λ is the length of a laser wave, Io is the intensity at the focal point (Z=0) for the fully absorbed sample and Leff is the effective thickness of the sample:

$$L_{eff} = \frac{1-e^{(-\alpha L)}}{\alpha} \quad (4)$$

Here, α is the linear absorption coefficient and L is the thickness of the object being studied. The nonlinear optical absorption coefficient (β) was determined from the open aperture curve.

$$\beta = \frac{2\sqrt{2}\,\Delta T}{I_0 L_{eff}} \quad (5)$$

It was found from the Z-scan experiment that the refractive index (n_2) of LOHCLs is 5.056 x 10^{-8} cm² W^{-1} and the nonlinear absorption coefficient (β) is 0.06 x 10^{-4} cm W^{-1}. Since n_2 is positive, the material guides light into its center as it gets brighter, causing rays of light to be focused by the same change in refractive index. Besides, since the Z-scan results are not symmetrical and the laser beam does not stop, thermo-optic effects are thought to be the main cause of nonlinearities. A thermo-optic process means that when light enters a material, the resulting heat modifies the refractive index around that point [22, 23]. Table 2 gives the measured third-order nonlinear susceptibility ($\chi^{(3)}$) of the LOHCL material.

3.8 Optimized Parameters

For the quantum-chemical study, the experimentally reported ionic form of L-ornithine hydrochloride, C5H13N2O2+·Cl−, was used as the starting model rather than a covalent C–Cl species [11, 12].

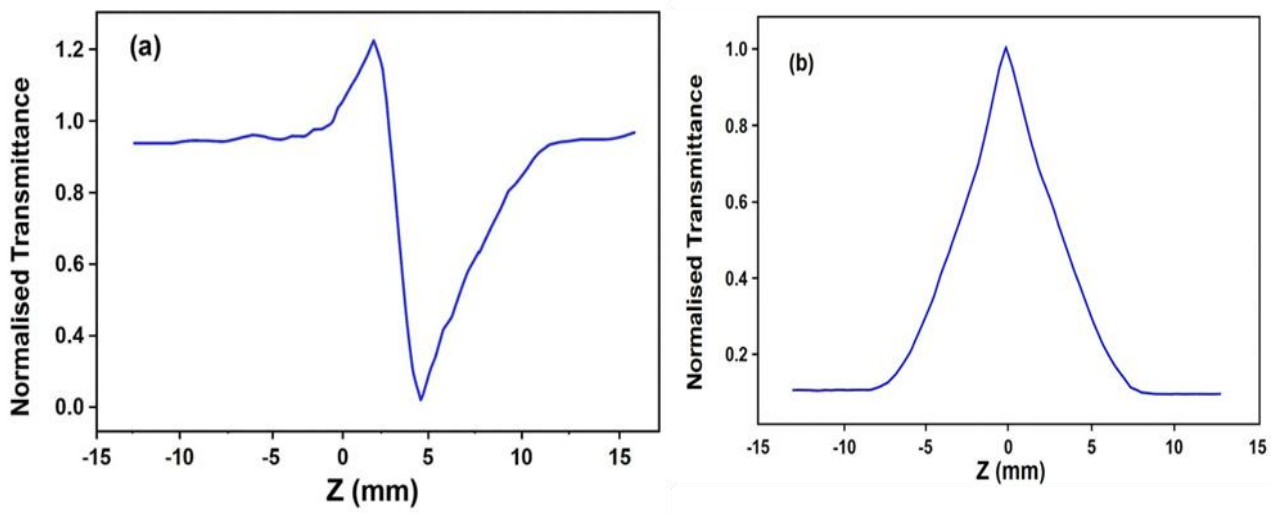

Figure 7. **(a)** Z-Scan curve of LOHCL in closed aperture (**b)** Z-Scan curve of LOHCL in open aperture

Table 2. Third order nonlinear optical properties of LOHCL crystal

Laser beam wave length (λ) = 532 nm
Laser Power (P) = 36 mW
Nonlinear refractive index (n_2) = 5.056 x 10^{-8} cm^2/W
Nonlinear absorption coefficient (β) = 0.06 x 10^{-4} cm/W
Absolute susceptibility ($\chi^{(3)}$) = 3.658 x 10-6 esu [electrostatic unit]

The optimized ion-pair geometry with atom numbering is shown in Figure 8, and the calculated structural parameters are listed in Table S1. The Cl1···H2 and H2···O16 contacts were found to be 1.923 Å and 1.040 Å, respectively. The C–C bond lengths lie in the range 1.40–1.55 Å. The calculated C–O bond length is 1.330 Å, shorter than a typical C–O single bond because of the carboxylate environment. The single-bond carbon distances are close to 1.47 Å, and the C–H bond lengths fall in the range 1.096–1.100 Å.

3.9 NBO Analysis

NBO analysis Combined with DFT/B3LYP/6-311++G (d,p) was used to examine the electronic structure present in LOHCL, in particular how orbital electrons transfer and keep their energy in a reaction. According to the results, oxygen atoms (nO) in the lone pairs often interact with the anti-bonding orbital and the interactions give stabilization energies of about 2.2 kJ mol^{-1}. Bringing together the lone pair orbital C_6-H_{18} of LOHCL and the anti-bonding orbital σ* ($C1_{22}$-H_{23}) forms O-H-Cl hydrogen bonding. These hydrogen bonds in the molecule have stabilization energy of 13.72 kJ mol^{-1}. These molecules are stabilized by both charge transfer interactions and hydrogen bonds within the LOHCL molecule. Based on NBO and second-order perturbation theory stabilization energies for all the bonds and interactions present in the LOHCL molecule have been calculated and are presented in Table S2. In general, the LOHCL is more stable because of the combined effect of hyperconjugation, hydrogen bonding, conjugation and charge transfer.

3.10 Frontier Molecular Orbital Analysis

The electron properties of LOHCL were studied using a FMO [Frontier molecular orbital] approach with DFT/B3LYP/6-311++G (d,p) calculations. FMOs rely on the close contact between HOMO [highest occupied molecular orbital] and LUMO [lowest unoccupied molecular orbital] which makes chemical reactions happen in compound formation by making the transition structure possible [1]. The HOMO is found on the C_3-H_{12}, N_2-H_{10}-H_{11}, C_1-O_8, O_9-H_{21}, H_{13}, H_{14}, Cl_{22} and H_{23} atoms of LOHCL, while the LUMO is placed on the N_2-H_{10}-H_{11}. Calculations showed that the separation between the highest and lowest energy levels is 3.00 eV (Figure 9). The HOMO-LUMO gap is low, probably owing to n-π* interactions which explains why intramolecular charge transfer is possible [24]. Nonlinear optical properties can be greatly influenced by the polarizability and dipole moment. A range of parameters relating to the reactivity of LOHCL were measured, including ionization potential (IP), electron affinity (EA), chemical potential (μ), overall energy balance (E), chemical hardness (η), electronegativity (χ), global softness (S), electrophilicity index (ω) and total energy change (ΔET) and are presented in Table 3.

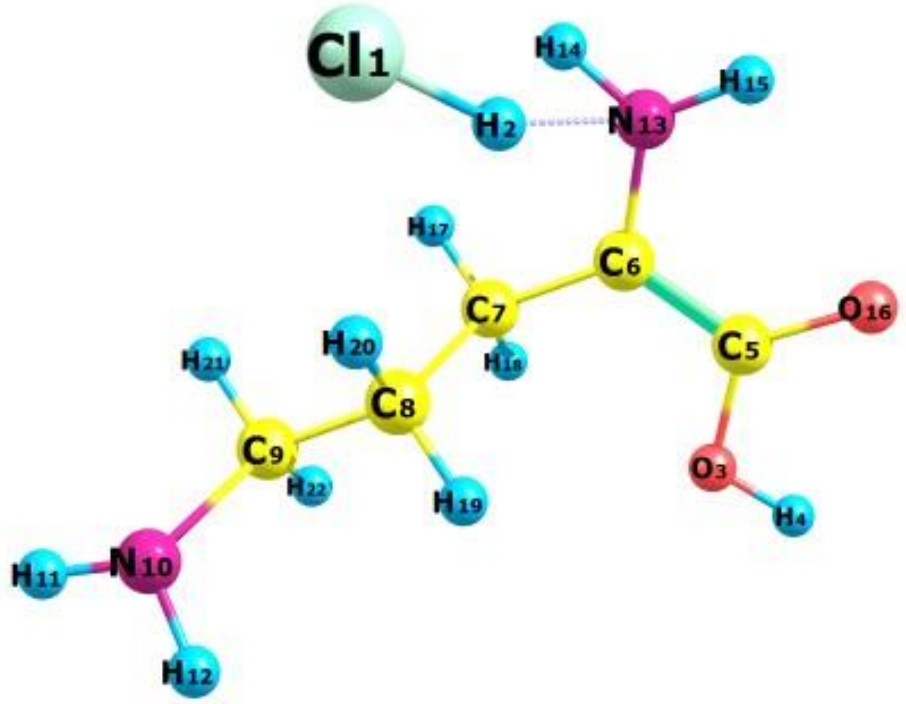

Figure 8. Optimized ion-pair model of LOHCL (C5H13N2O2+·Cl−)

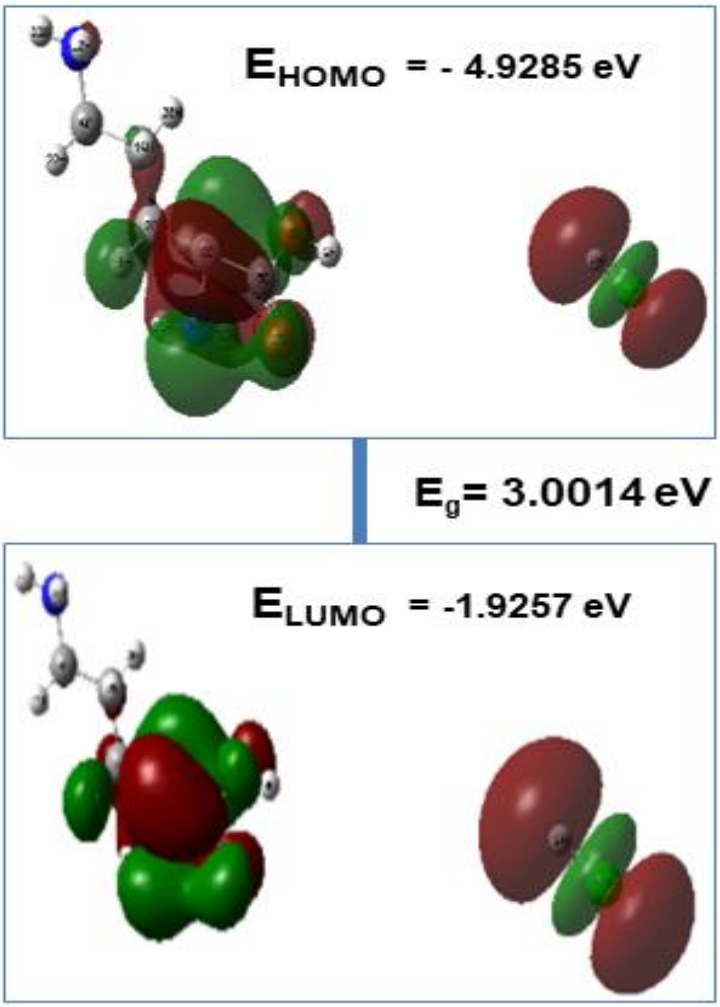

Figure 9. Frontier molecular orbitals of LOHCL

Table 3. Molecular orbital properties of LOHCL

Parameters	B3LYP/6-311++G(d,p)
HOMO energy, E_{HOMO} (eV)	-4.928
LUMO energy, E_{LUMO} (eV)	-1.927
HOMO- LUMO energy gap, ΔE_{GAP} (eV)	3.00
Ionisation potential, IP (eV)	4.928
Electron affinity, EA (eV)	1.927
Electronegativity, χ (eV)	3.4275
Chemical hardness, η (eV)	1.5005
Global softness, S $(eV)^{-1}$	0.3332
Chemical potential, μ (eV)	-3.4275
Electrophilicity index, ω (eV)	3.92

3.11 MEP Analysis

Molecular electrostatic potential (MEP) calculations are done to reveal the ways in which the LOHCL molecule might interact or react. An analysis of electron density with MEP can explain a molecule's tendency to react to other compounds. An iso surface was created using MEP values from -0.208e0 for red to +0.208e0 for the deepest blue. In Figure 10 LOHCL's reactivity pattern for electrophiles and nucleophiles is illustrated. Showing that the best results would be found in the red zone. The oxygen group in the LOHCL is where the electrophilic reactions occur. Because some nuclear charge density is shielded by substituents, the hydrogen atoms in the LOHCL molecule dominate its nucleophilic reactivity and the blue zone means the strongest repulsive force. Partial protection of the positive nuclear charge is possible when the amino group is surrounded by electrons [25]. In practice, MEP analysis reveals where nucleophiles and electrophiles might target the molecule, supporting efforts to determine how LOHCL will respond to other substances.

3.12 Thermodynamic Properties

DFT, HF and a set of basic functions were used to study the thermodynamics of LOHCL. Calculations were performed for parameters such as the zero-point vibrational energy (ZPVE), thermal energy, specific heat capacity and entropy. The measured ground state values at 273 K are included in Table S3 for reference. ZPVE, which represents the vibrational energy of a molecule at absolute zero temperature, exhibited significant variations depending on the chosen computational method and basis set. In general, the HF method yielded higher ZPVE values compared to DFT calculations. The dipole moment, a measure of a molecule's polarity and indicative of its charge distribution, also displayed a dependence on the selected method and basis set. Finding the direction of a molecule's dipole-moment depends on where the positive and negative charges are in the molecule. The values of dipole moments are fixed for neutral molecules. The selected origin and alignment of the molecules affect the electric dipole moments in charged systems. In every case, HF and DFT with B3LYP wave functions find that the structure linked to HF/6-31++G (d,p) has the highest dipole moment and the one linked to B3LYP/6-31++G(d,p) shows the lowest. The high dipole moment gives high intermolecular charge transfer which gives very good NLO properties. It was also determined how the heat capacity (C) and entropy (S) of the LOHCL molecule change as the temperature moves between 100 and 600 K. Following expectations, the values of C and S grows as the temperature rises. The rising impact of vibrational modes on the molecular energy at higher temperatures is the reason for this trend [26].

3.13 Mulliken Charge Analysis

The Mulliken charges that influence how charges are distributed on atoms are shown in both Table S4 and Figure 11 and are very important for explaining dipole moment, polarizability and electron structures. It is important to acknowledge that these charges can vary depending on the chosen computational method (HF or DFT) and basis set. This variation likely arises from fundamental differences in how each method accounts for electron polarization within the molecule. Interestingly, the analysis revealed a consistent trend across both HF and DFT methods: a decrease in the calculated charge on the C_1, N_2, C_3, C_4, C_5 atom and Increase in the calculated charge on the C_6, N_7, O_9 atom. Hydrogen atom consistently exhibits a positive charge in all calculations.

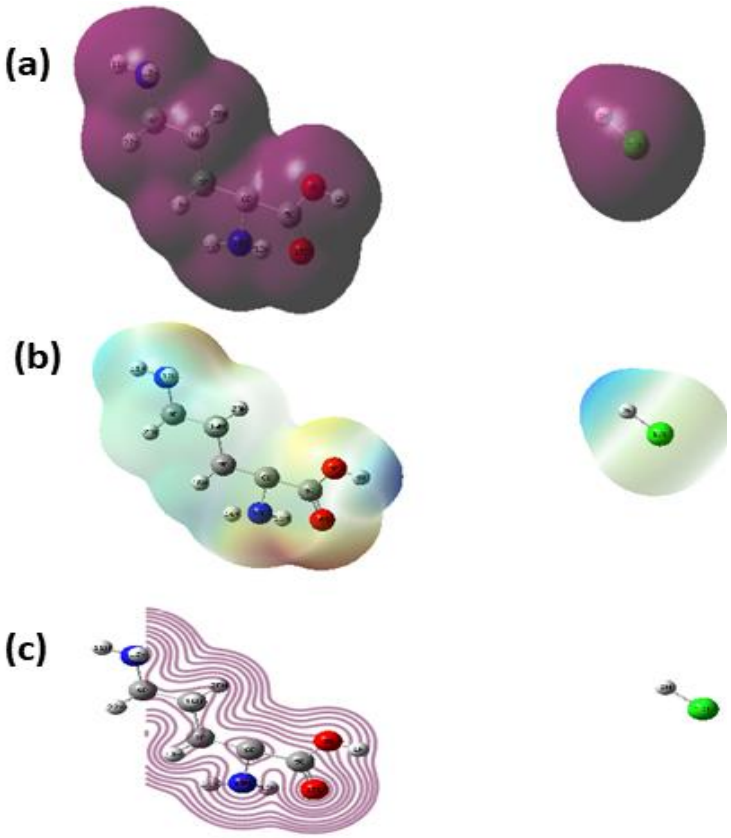

Figure 10. (a) Shows the distribution of charge in the molecule LOHCL **(b)** illustrates the total electron density map and **(c)** has a contour map of the total electron density.

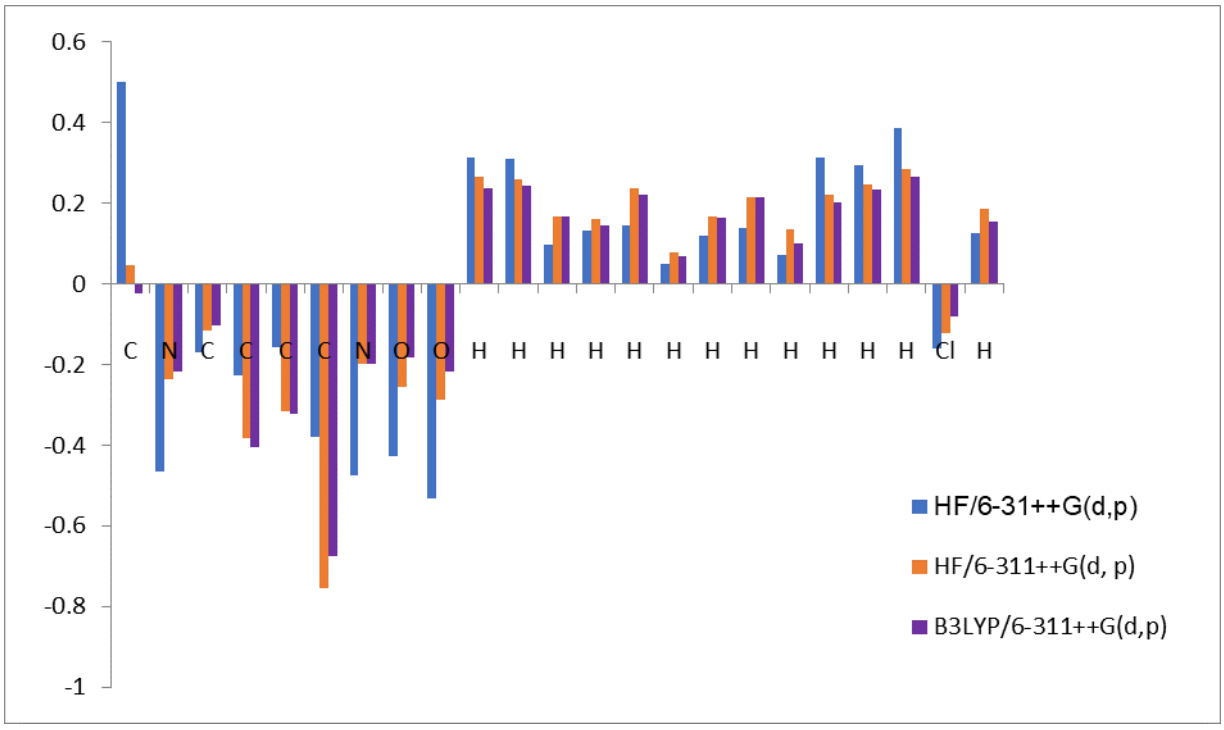

Figure 11. Mullikan's Atomic charges between theoretical (HF and DFT) approaches.

This result follows the commonly observed trend in which carbon atoms, functioning as electron-donating centres, exhibit negative Mulliken charge values, whereas hydrogen atoms, acting as electron-accepting species, carry positive charges. It was also observed that the B3LYP approach produced comparatively larger absolute charge values than the HF method, indicating methodological differences in the predicted electronic charge distribution.

4. Conclusion

In this work, L-ornithine monohydrochloride crystals were successfully grown using the slow-evaporation method and evaluated through an integrated set of structural, spectroscopic, thermal, quantum-chemical and nonlinear-optical analyses. X-ray diffraction analysis confirmed the formation of the reported monoclinic LOHCL phase with good crystalline integrity. The optical studies demonstrated excellent transparency throughout the visible region with a cut-off around 223 nm, while photoluminescence measurements revealed blue emission at 474 nm. Thermal studies indicated that the crystal maintains stability up to about 255 °C, indicating adequate resistance for moderate-temperature device environments. The measured Z-scan parameters, including a positive nonlinear refractive index and finite nonlinear absorption coefficient, establish the presence of third-order nonlinear optical activity in LOHCL. Complementary DFT calculations supported the experimental observations by clarifying the optimized ionic structure, frontier orbital distribution, charge-transfer characteristics, Mulliken charge profile and thermodynamic behaviour; the calculated HOMO-LUMO separation of 3.00 eV further suggests feasible electronic polarization under optical excitation. Overall, the study does not claim a new crystal phase, but it provides a consolidated structure-property assessment of a known amino-acid hydrochloride salt using coordinated experimental and theoretical tools. These findings position LOHCL as a promising candidate for further investigation in optical switching, photonic modulation and related nonlinear-optical applications, provided that future work expands device-level validation and comparative performance analysis.

References

[1] M. Shkir, S. AlFaify, H. Abbas, G. Bhagavannarayana, A physico-chemical approach to study the experimental and theoretical properties of l-ornithine monohydrochloride: an organic nonlinear optical material. Materials Chemistry and Physics, 155, (2015) 36-46. https://doi.org/10.1016/j.matchemphys.2015.01.062

[2] Q. Hu, X. Yu, H. Liu, J. Qiu, W. Tang, S. Liang, L. Li, M. Du, J. Jia, H. Ye, Tunable Organic ENZ Materials with Large Optical Nonlinearity. ACS Photonics, 10(10), (2023) 3612–3620. https://doi.org/10.1021/acsphotonics.3c00675

[3] L.R. Dalton, Organic electro-optic materials: theory and experiment, devices, and applications [Invited]. Optical Materials Express, 15(8), (2025) 2037. https://doi.org/10.1364/ome.567555

[4] B. Korkmaz, S. Agtas, B. Sütay, E. Yildirim, I. Yilgor, M. Yurtsever, B.F. Senkal, Y. Gursel, Influence of hydrogen bond on the mesomorphic behaviour in urethane based liquid crystalline compounds: Experimental and computer simulation study. Journal of Molecular Liquids, 317, (2020) 114001. https://doi.org/10.1016/j.molliq.2020.114001

[5] A. Ullah, M. Ibrahim, A. Yousuf, M.A. Ali, H. Xu, M. Arshad, Crafting optical wonders: The interplay of electron push–pull dynamics and π-conjugation in non–linear optics. Next Materials, 9, (2025) 101239. https://doi.org/10.1016/j.nxmate.2025.101239

[6] S. Lakshmi, M. Saravanan, Synthesis, crystal structure, optical, spectroscopic, and self-defocusing properties of novel 2-amino 6-methyl pyridinium adipate adipic acid (2A6MPAA) single crystals for third harmonic nonlinear optical applications. Optical Materials, 149, (2024) 114892. https://doi.org/10.1016/j.optmat.2024.114892

[7] G. Sangeetha, S. Ramalingam, G. Susithra, Interplay of crystal structure, electronic delocalization, and nonlinear optical response in sodium 4-nitrobiphenyl-4-olate salt: An integrated experimental–computational approach. Physica B Condensed Matter, 734, (2026) 418630. https://doi.org/10.1016/j.physb.2026.418630

[8] I. Irshad, M. Ishaq, M. Umar, I.A. Khan, Evaluation of electronic, optoelectronic, and nonlinear optical responses in functionalized pyrazine chromophores: a Density Functional Theory study. Energy Technology, 14(3), (2026) e202502125. https://doi.org/10.1002/ente.202502125

[9] W. Ji, B. Xue, Z.A. Arnon, H. Yuan, S. Bera, Q. Li, D. Zaguri, N.P. Reynolds, H. Li, Y. Chen, S. Gilead, S. Rencus-Lazar, J. Li, R. Yang, Y. Cao, E. Gazit, Rigid tightly packed amino acid crystals as functional supramolecular materials. ACS Nano, 13(12), (2019) 14477–14485. https://doi.org/10.1021/acsnano.9b08217

[10] D. Sajan, H. Ravindra, N. Misra, I.H. Joe, Intramolecular charge transfer and hydrogen bonding interactions of nonlinear optical material N-benzoyl glycine: Vibrational spectral study. Vibrational Spectroscopy, 54(1), (2010) 72–80. https://doi.org/10.1016/j.vibspec.2010.06.007

[11] A. Chiba, T. Ueki, T. Ashida, Y. Sasada, M. Kakudo, The crystal structure of L-ornithine hydrochloride. Acta Crystallographica, 22(6), (1967) 863-870. https://doi.org/10.1107/S0365110X67001690

[12] B. Dittrich, P. Munshi, M.A. Spackman, Redetermination, invariom-model and multipole refinement of L-ornithine hydrochloride. Structural Science, B63(3), (2007) 505-509. https://doi.org/10.1107/S0108768107014838

[13] K.K. Jha, B. Gruza, P. Kumar, M.L. Chodkiewicz, P.M. Dominiak, TAAM: a reliable and user friendly tool for hydrogen-atom location using routine X-ray diffraction data. Structural Science, 76(3), (2020) 296-306. https://doi.org/10.1107/S2052520620002917

[14] T. Balakrishnan, K. Ramamurthi, Crystal growth, structural, optical, mechanical and thermal properties of a new nonlinear optical single crystal: l-Ornithine monohydrochloride. Spectrochimica Acta Part A: Molecular and Biomolecular Spectroscopy, 72(2), (2009) 269-273. https://doi.org/10.1016/j.saa.2008.09.030

[15] M. Nageshwari, C.R.T. Kumari, P. Sangeetha, G. Vinitha, M.L. Caroline, Third order nonlinear optical, spectral, dielectric, laser damage threshold, and photo luminescence characteristics of an efficacious semiorganic acentric crystal: L-ornithine monohydrochloride. Chinese Journal of Physics, 56(2), (2018) 502-519. https://doi.org/10.1016/j.cjph.2018.02.003

[16] M. Sagir, K. Mushtaq, M. Khalid, M. Khan, M.B. Tahir, A.A. Braga, Exploration of linear and third-order nonlinear optical properties for donor–π-linker–acceptor chromophores derived from ATT-2 based non-fullerene molecule. RSC Advances, 13(45), (2023) 31855-31872. https://doi.org/10.1039/D3RA04580C

[17] M. Khadka, M. Sah, R. Chaudhary, S.K. Sahani, K. Sahani, B.K. Pandey, D. Pandey, Spectroscopic, quantum chemical, and topological calculations of the phenylephrine molecule using density functional theory. Scientific Reports, 15(1), (2025) 208. https://doi.org/10.1038/s41598-024-81633-2

[18] S.A. Halim, A.B. El-Meligy, A.M. El-Nahas, S.H. El-Demerdash, DFT study, and natural bond orbital (NBO) population analysis of 2-(2-Hydroxyphenyl)-1-azaazulene tautomers and their mercapto analouges. Scientific Reports, 14(1), (2024) 219. https://doi.org/10.1038/s41598-023-50660-w

[19] A. Pawlukojć, K. Hołderna-Natkaniec, G. Bator, I. Natkaniec, INS, IR, RAMAN, 1H NMR and DFT investigations on dynamical properties of l-asparagine. Vibrational Spectroscopy, 72, (2014) 1-7. https://doi.org/10.1016/j.vibspec.2014.02.002

[20] M. Shkir, B. Riscob, M. Hasmuddin, P. Singh, V. Ganesh, M.A. Wahab, E. Dieguez, G. Bhagavannarayana, Optical spectroscopy, crystalline perfection, etching and mechanical studies on P-nitroaniline (PNA) single crystals. Optical Materials, 36(3), (2014) 675-681. https://doi.org/10.1016/j.optmat.2013.11.009

[21] B. Mohanbabu, R. Bharathikannan, G. Siva, Synthesis, growth, spectral, third order nonlinear optical and antimicrobial behaviour of 5-bromopyridine-4-hydroxybenzoic acid single crystals. Journal of Optoelectronics and Advanced Materials, 17(11-12), (2015) 1603-1614.

[22] E. Shobhana, B. Balraj, B. Mohanbabu, V. Sathyanarayanamoorthi, A Review on the Non-Linear Optical Performance of Picric Acid based Crystals. Asian Journal of Chemistry, 35(11), (2023) 2603-2617.

[23] J. Hu, J. Wu, D. Jin, S.T. Chu, B.E. Little, D. Huang, R. Morandotti, D.J. Moss, Thermo-optic response and optical bistablility of integrated high-index doped silica ring resonators. Sensors, 23(24), (2023) 9767. https://doi.org/10.3390/s23249767

[24] S.A. Siddiqui, M.M. Abdullah, Molecular modeling and simulation of some efficient charge transfer materials using density functional theory. Materials Today Communications, 22, (2020) 100788. https://doi.org/10.1016/j.mtcomm.2019.100788

[25] Hélène, G. Lancelot, Interactions between functional groups in protein-nucleic acid associations. Progress in Biophysics and Molecular Biology, 39, (1982) 1-68. https://doi.org/10.1016/0079-6107(83)90013-5

[26] D.E. Moreno, C.Z. Hargather, Thermodynamic Properties as a Function of Temperature of AlMoNbV, NbTaTiV, NbTaTiZr, AlNbTaTiV, HfNbTaTiZr, and MoNbTaVW Refractory High-Entropy Alloys from First-Principles Calculations. Solids, 4(4), (2023). https://doi.org/10.3390/solids4040021

Authors Contribution Statement

N. Saranya: Conceptualization, methodology, data collection, formal analysis, and writing the original draft. R. Karunathan: Conceptualization, validation, supervision, and writing the original draft. P. Vidhya: Writing, review, and editing. S. Bhuvaneswari: Writing, review, and editing. All the authors read and approved the final version this manuscript.

Funding

The authors declare that no funds, grants or any other support were received during the preparation of this manuscript.

Competing Interests

The authors declare that there are no conflicts of interest regarding the publication of this manuscript.

Data Availability

The data supporting the findings of this study can be obtained from the corresponding author upon reasonable request.

Has this article screened for similarity?

Yes

About the License